

Differentiate Thermal Property of Mammary Glands for Precise Photothermal Therapy

Yuxin Fang, Weijie Zheng, Yuxuan Peng, Jianhua Liu, Jianshu Gao, Yi Tu, Shengrong Sun, Xiaona Huang, Jinjuan She,* Chuang Chen,* Shen Xu, and Yanan Yue*

As an alternative to conventional methods, photothermal therapy is promising in breast cancer therapy. It is essential to prevent overheating of normal tissues and underheating of target tissues, which strongly depends on thermal transport processes. In this work, for the first time, the thermal properties of mammary glands in pubertal and mature mice is accurately measured. Thermal conductivity of mammary gland in pubertal mice is measured as $0.19^{+0.005}_{-0.005} \text{ W m}^{-1} \text{ K}^{-1}$, slightly higher than that of fat ($0.17 \text{ W m}^{-1} \text{ K}^{-1}$), which is the main component of connective tissue in mammary glands. However, with the growth and pregnancy of mature mice, thermal conductivity of mammary gland increases to $0.32^{+0.004}_{-0.004} \text{ W m}^{-1} \text{ K}^{-1}$, 66.84% higher than that of pubertal mice. Numerical simulations are conducted to understand the role of thermal conductivity in photothermal therapy. The maximum temperatures in mammary glands of pubertal and mature mice are 49.6 and 44.6 °C, respectively, under the same laser irradiation conditions. This implies that higher thermal conductivity in mature mice mammary glands might lead to ineffectiveness in reaching to the desired temperature. This work suggests that age and pregnancy affect the thermal properties of mammary glands which are not negligible in breast cancer photothermal therapy.

1. Introduction

Breast cancer (BC) is the most common malignant tumor in women worldwide according to the data from Global Cancer Observatory.^[1,2] Traditional treatments of BC, including surgery,^[3] radiotherapy,^[4] and chemotherapy^[5] are difficult to eradicate BC stem cells, which are responsible for tumor dissemination and metastasis.^[6,7] A new therapeutic method, photothermal therapy, is applied to patients who are not suitable for traditional treatments due to their physical conditions and their concerns about side effects.^[8,9] Photothermal therapy employs photothermal agents to convert optical energy into thermal energy at a specific wavelength.^[10,11] It has attracted wide attention due to advantages such as minimal side-effect,^[12] simple operation,^[13] high temporal-spatial resolution,^[14] and low toxicity to normal tissues.^[15] Photothermal therapy has been regarded as one of the most promising techniques that could be applied to the treatment of BC.^[16]

In photothermal therapy, the target areas require to be kept at a temperature range between 41 and 47 °C for tens of minutes or higher temperature for a shorter time under laser irradiation.^[17] High-temperature rise could cause irreversible damage to normal cells, while low temperature (<40 °C) could not ablate tumor cells effectively in a short time. It is vital to improve the efficiency and accuracy of treatment and avoid unwanted thermal damage to the healthy tissue, especially in clinical application. The direct measurement of heat transfer in photothermal therapy is often difficult due to access and practical measurement issues, then analytical or numerical methods could be valuable alternatives in allowing us to predict the outcome of heat transfer procedure. The reliability of predictions depends on employing an appropriate heat transfer model and accurate thermal conductivity of mammary gland. The accurate knowledge of the thermal conductivity is essential to understand the heat transfer mechanisms, which could facilitate the development of realistic time-dependent thermal models and reasonable parameter settings in BC hyperthermia.


One of the first techniques used to measure thermal conductivity of biological tissues was the guarded hot plate method, which is a 1D heat flow model and based on a steady-state process.^[18,19] Longer exposure can change the basic structure of tissue and

Y. Fang, Y. Peng, J. Gao, X. Huang, Y. Yue
Key Laboratory of Hydraulic Machinery Transients (MOE)
School of Power and Mechanical Engineering
Wuhan University
Wuhan 430072, China
E-mail: yyue@miamioh.edu

W. Zheng, J. Liu, Y. Tu, S. Sun, C. Chen
Department of Breast and Thyroid Surgery
Renmin Hospital of Wuhan University
Wuhan 430060, China
E-mail: chenc2469@163.com

J. She, Y. Yue
Department of Mechanical and Manufacturing Engineering
Miami University
OH 45056, USA
E-mail: jshe@miamioh.edu

S. Xu
School of Mechanical and Automotive Engineering
Shanghai University of Engineering Science
Shanghai 201620, China

 The ORCID identification number(s) for the author(s) of this article can be found under <https://doi.org/10.1002/adtp.202100216>

DOI: 10.1002/adtp.202100216

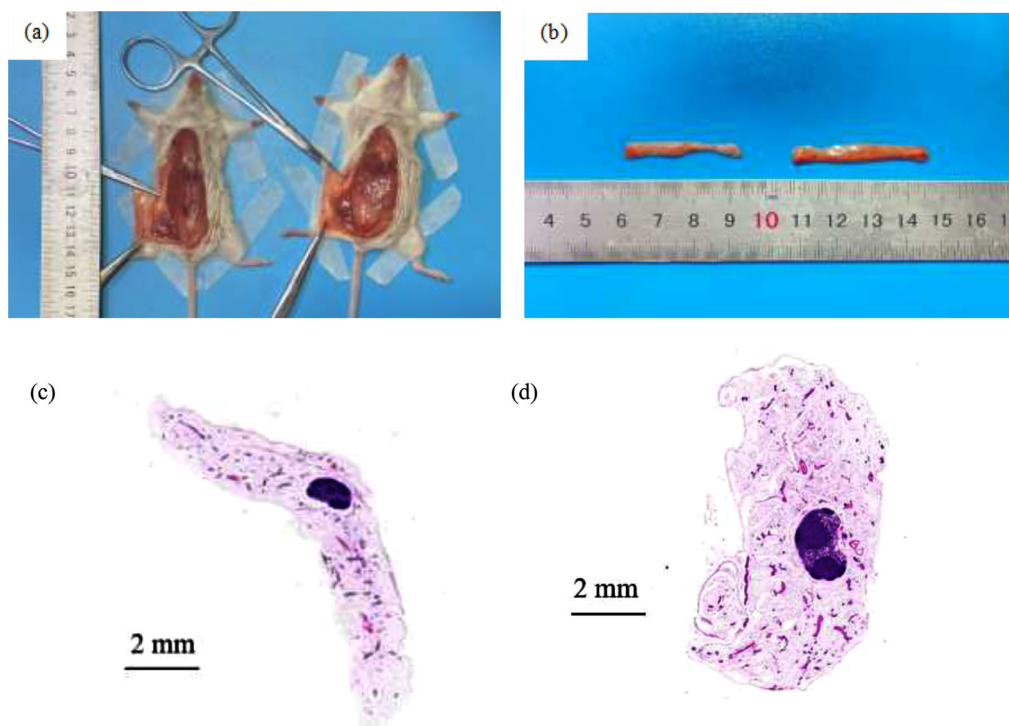


Figure 1. a) Anesthetized pubertal mouse (left) and mature mouse (right). b) The mobilized mammary gland of pubertal mouse (left) and mature mouse (right). c) The mammary gland H-E stained section of pubertal mice. d) The mammary gland H-E stained section of mature mice.

increase water loss resulting in inaccurate values.^[20] The laser flash method is a noncontact and transient optical technique,^[21] but it assumes the sample to be a blackbody with a layer of black coating on the sample surface^[22] which is unsuitable for biomaterials. The cut-bar and embedded thermistor method can measure the thermal conductivity of biomaterials, but it requires sample to have at least ≈ 10 mm thickness.^[23] The thermal conductivity of swine left ventricle in normal and ablated conditions has been obtained by this method *ex vivo*.^[24] The thickness of the mammary gland is only about 2 mm, which requires the method to measure the thermal conductivity of thin-film material. The three-omega method is common in measuring the thermal conductivity of thin materials.^[25] But the requirement of obtaining the temperature coefficient of resistance in advance limits its application in measuring mammary gland thermal conductivity.^[26] Above methods have strict requirements for the tested sample size or need complex numerical analysis to obtain results. It is challenging to find a suitable method to measure the thermal conductivity of the mammary gland with a small size.

The customized hot wire method is used in this paper to study the thermal conductivity of mammary glands. Sample preparation is described in Section 2. The theory and governing equations for the simplified analysis are given in Section 3. Subsequent experiments conducted on the mammary glands of pubertal and mature mice are described in Section 4 to uncover the effective thermal transport in mammary glands. In Section 5, numerical simulations are conducted to understand the role of thermal properties in photothermal therapy. Under the same irradiation conditions, the effective treatment areas of pubertal and ma-

ture mice mammary glands are different. It shows that the effect of pregnancy and age on the thermal conductivity of mammary glands could not be ignored in BC photothermal therapy.

2. Sample Preparation

2.1. Ethics Statement

All animal studies are reviewed and approved by the Laboratory Animal Welfare & Ethics Committee (IACUC) of Renmin Hospital of Wuhan University (Issue No. 20200702). All animals are housed in sterilized plastic cages under pathogen-free conditions (21–25 °C, 12/12 light/dark cycle). Food and water are offered *ad libitum*. The animals are euthanized using CO₂ overdose followed by cervical dislocation to ameliorate their suffering.

2.2. Preparation Details

The female Balb/c mice are anesthetized with 1% pentobarbital sodium injected intraperitoneally (30 mg Kg⁻¹). After the mice are well anesthetized, the limbs are secured, and the abdominal skin is sterilized. An incision is made on the abdomen to expose and dissect the inguinal gland within 5 min. The measurement of thermal conductivity is conducted subsequently, and then the mice are euthanized. All animals are monitored with pulse and breath and are placed on the warming pad for temperature control during anesthesia. As shown in **Figure 1a**, the anesthetized pubertal Balb/c mouse (left) is about 9.50 cm in length and the

average weight of pubertal mice is 22–25 g. The mature mouse (right) is about 10 cm in length and the average weight of mature mice is 28–32 g. The mammary glands are close to the skin, which is beneficial to conduct laser irradiation for photothermal therapy. The mammary gland in the pubertal mice mobilized by blunt dissection is presented in Figure 1b, which is 3.20 cm in length, 0.35 cm in width, and 0.20 cm in thickness. The mammary gland in the mature mouse is about 3.7 cm in length and 0.40 cm in width. After the measurement, the mammary glands are fixed in 10% formalin-buffered acetate, dehydrated, and embedded in paraffin. The embedded specimens are cut into 5 μm serial sections, stained with hematoxylin-eosin, then dehydrated and viewed under the microscope Figure 1c,d.

The inguinal gland is dissected, spread out on glass slides, and fixed in Carnoy's fixative (VibroView™ Cat. No. VB-300) for 2–4 h at room temperature. The slides are washed with alcohol/distilled water gradually, starting with 70% ethanol for 30 min, and then rinsed in distilled water for 5 min. Then, the mammary gland is stained in carmine alum (VibroView™ Cat. No. VB-300) at room temperature overnight. Next, the samples are washed in 70%/95%/100% EtOH for 15 min per time orderly. Samples are cleaned with three changes of xylene (10 min per change) and photographically documented.

To intuitively compare the mammary ductal architecture of the two kinds of mice, a 50 μL Hamilton syringe affixed with a 33 G metal hub needle is used to inject 1% methylene blue (a dye widely applied clinically) into the mammary ducts through the opening of nipple. The detailed procedure is as followings. BALB/c mouse is anesthetized with a mix of isoflurane and oxygen using a chamber to rapidly induce anesthesia, then maintain it by switching the mouse under the stereoscope with a mask for drug delivery. After securing its extremities and sterilizing the skin on the inguinal gland, the mouse is injected 20 μL methylene blue through the nipple opening to fill the entire ductal tree.^[27] Lastly it is euthanized and dissected to expose the dyed mammary gland for photographical documentation.

3. Measurement Method

3.1. Principle

As mentioned above, the mammary glands' small size and thin thickness limit the choice of thermal conductivity measurement methods. Based on the principle of the transient 1D heat conduction,^[28] the hot wire introduces a thermal pulse for a finite time with a constant heating power and generates cylindrical coaxial isotherms initially at equilibrium. The temperature distribution is sensitive to the radial heat flow and thermal properties of mammary glands, which is defined by the governing equation

$$\frac{\partial^2 T}{\partial r^2} + \frac{1}{r} \frac{\partial T}{\partial r} = \frac{1}{\alpha} \frac{\partial T}{\partial t} \quad (1)$$

where T is the temperature at position r and time t , α is the thermal diffusivity. The initial and boundary conditions are $T = T_0$ at $t = 0$ and $q = -2\pi kr \partial T / \partial r$ for $t > 0$. Finally, the thermal conductivity can be obtained by the fundamental equation as^[4]

$$k = \frac{q}{4\pi} / \frac{\partial T}{\partial \ln t} \quad (2)$$

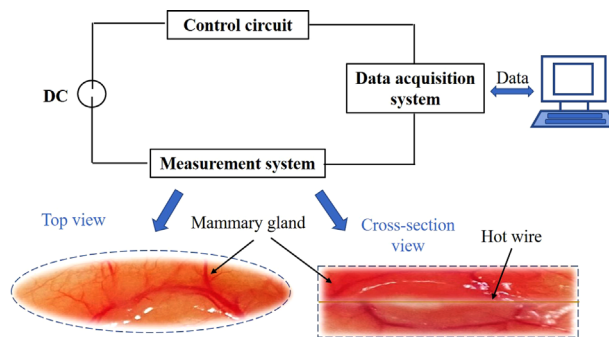


Figure 2. Simplified system diagram of experimental measurement.

As illustrated in Figure 2, the whole experiment system comprises the measurement system, data acquisition system, and control circuit. The data acquisition can record voltage data at the rate of 1000 samples s^{-1} simultaneously from all channels, which could ensure the accuracy of the logged data. A current source with 1 mV resolution is utilized to supply a constant voltage in the measurement system. The specially treated hot wire monitors its own temperature while generating heat gradient in the mammary glands, acting as a temperature source and sensor. The mathematical modeling error mainly results from the deviation between the measuring apparatus and the theoretical 1D heating model.

Previous studies indicated that L/D ratio must be greater than 25 to minimize the axial heat loss through hot wire, and the model could be taken as infinitely long.^[29] The effective length of the hot wire ($L = 1.5$ cm) and radius ($r_1 = 15$ μm) in this measurement meet the requirements to reduce the error in the mathematical model. The thermal conductivity could be derived through fitting the voltage–time line

$$k = \frac{E^3 R_0^2 R \alpha_1}{4\pi L (R_0 + R)^4} / \frac{dU}{d \ln t} \quad (3)$$

where E is the applied constant voltage. $\alpha_1 = 0.00386$ K^{-1} is the temperature coefficient of the hot wire.^[30] L is the effective length of the hot wire. R and R_0 are the resistance in the circuit. U is voltage of hot wire which changes with the resistance. $dU/d \ln t$ is the slope obtained from the linear region of voltage and logarithmic time plot which can be recorded by data acquisition. The minimum time requires to achieve a linear relationship is estimated by $r_1^2 / 4\alpha t < (0.16)^2$, where r_1 is 15 μm and α is 10^{-7} – 10^{-6} $\text{m}^2 \text{s}^{-1}$ in this measurement.^[31] According to the above equations, the thermal conductivity can be determined from the voltage and logarithmic time plot.

Since the air between the sample and hot wire will lower the accuracy of the measurement results, it is critical to exclude the residual air and keep the mammary glands in good contact with the hot wire in this experiment. The mammary gland is lightly pressed using a small clamp to minimize contact resistance. Besides, controlling the measurement time and monitoring the temperature rise is vital in this experiment. The prolonged exposure would change the tissue's basic structure, resulting in large errors in the measured thermal conductivity. Thus, the sample is exposed to the environment for up to 3 min, and surrounding

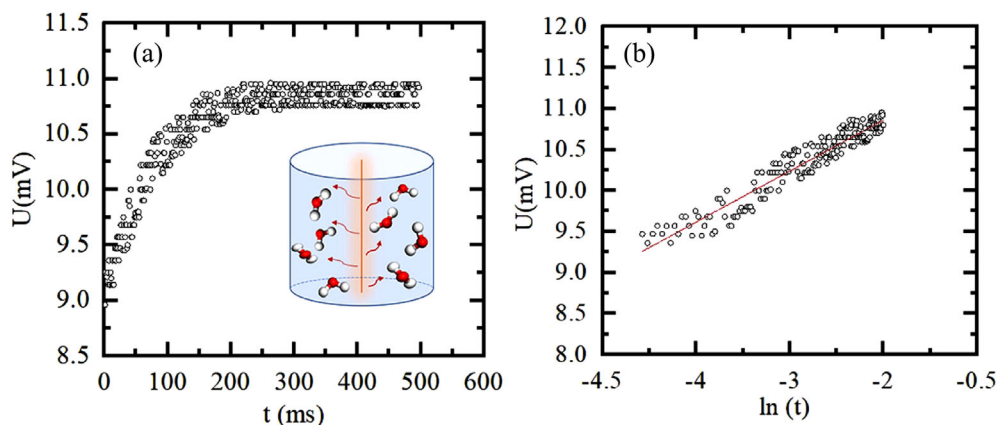


Figure 3. a) Voltage variation against time in deionized water. b) Voltage varies with logarithmic time.

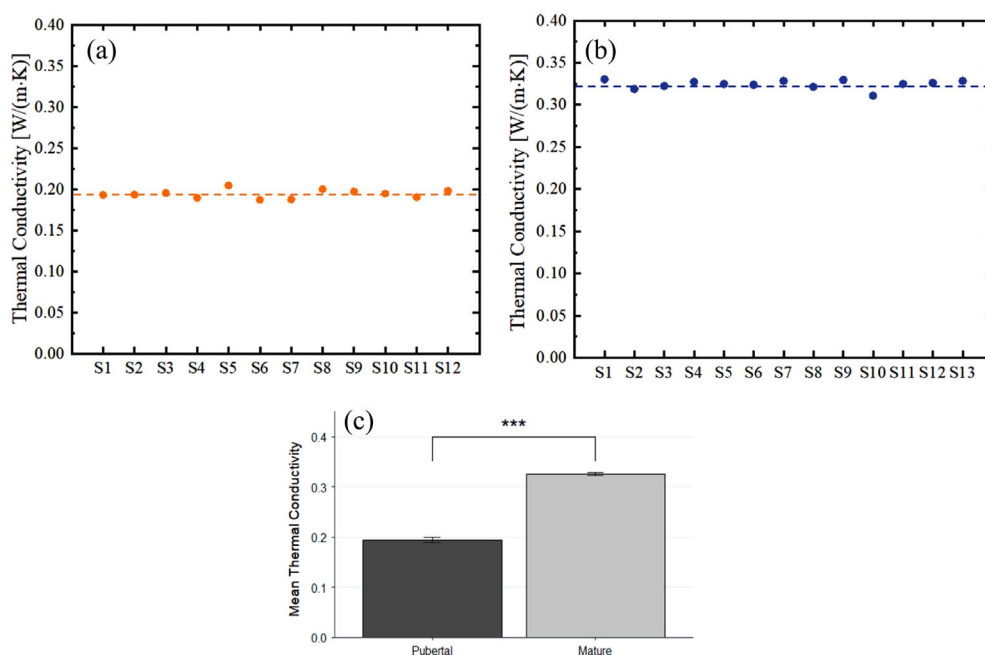


Figure 4. a) Measured thermal conductivity of mammary gland in pubertal mice. b) Measured thermal conductivity of mammary gland in mature mice. c) Mean and standard deviation of thermal conductivity of mammary gland in pubertal mice (12 samples) and mature mice (12 samples). “***” indicates the difference is statistically significant at 0.001 level with the ANOVA test.

temperature and humidity is kept constant during each measurement.

3.2. Measurement Details and Verification

The accuracy of the customized experimental equipment is calibrated before the mammary gland measurement. Deionized water is employed as a standard material with thermal conductivity of $0.61 \text{ W m}^{-1} \text{ K}^{-1}$.^[32] **Figure 3a,b** shows the voltage varies with time and logarithmic time in destined water. A linear relationship between temperature and logarithmic time is determined when the measurement time is sufficiently long. The measurement is repeated four times, and the result is $0.62^{+0.005}_{-0.005} \text{ W m}^{-1} \text{ K}^{-1}$, which

confirms the feasibility of the measurement method and verifies the accuracy of the equipment for measuring the thermal conductivity of conductive materials.

4. Experimental Results and Discussion

4.1. Statistical Analysis

Adapting the same method, thermal conductivity of mammary glands for different mice is measured as shown in **Figure 4a,b**. Before analysis, the experimental data were processed in Excel to calculate thermal conductivity for each sample by using Equation (3) as discussed in Section 3.1. In total, 25 individual thermal

Table 1. ANOVA Test summary and mean and standard deviation of each type of the mice.

Factor	F-statistics	df	P-value	Partial η^2
Mouse type	5235	(1,22)	<0.001	0.99
Mean \pm SD	Mature: 0.32 ± 0.004		Pubertal: 0.19 ± 0.005	

conductivities were obtained: 12 for pubertal samples and 13 for mature samples. All were analyzed using statistical techniques in R Studio.

To test the differences of thermal conductivity in mature versus pubertal mice, a one-way analysis of variance (ANOVA) was performed with the derived thermal conductivity as the dependent variable, mouse type (pubertal or mature) as the between-subject factor. The initial assumption checked identified sample #10 in mature mice as an outlier and therefore it was removed in analysis, which led to 12 samples in each type of mice. Further Shapiro–Wilk test of normality on the dataset without the outlier showed that the data was normally distributed (p -value = 0.809 > 0.05). In addition, Levene's test of homogeneity indicated that there were no differences in variances of both groups (p -value = 0.243 > 0.05). Therefore, the dataset met the assumptions of ANOVA test. Results were summarized in Figure 4c and Table 1. It is obvious that mature mice has a significantly higher thermal conductivity than pubertal mice (0.32 ± 0.004 vs 0.19 ± 0.005 , $F(1,22) = 5235$, p -value < 0.001), and the effect size is large (Partial $\eta^2 = 0.99 > 0.14$).

From the analysis above, the average thermal conductivity of the mammary gland in pubertal mice is obtained as $0.19^{+0.005}_{-0.005}$ W m⁻¹ K⁻¹, which is close to the thermal conductivity of fat cells 0.17 W m⁻¹ K⁻¹.^[33] Similarly, the average thermal conductivity for mature mice is $0.32^{+0.004}_{-0.004}$ W m⁻¹ K⁻¹, which increases 66.80% compared to that of the pubertal mice. The change in thermal properties is reasonable considering the variation in the microstructure of the mammary glands. Previous studies revealed that pregnancy and breastfeeding have a dual effect on the development of BC. Hackman and Kugel^[34,35] conducted experiments on mammary glands' genes during lactation and nonlactation. The results revealed that the morphology and function of mammary glands drastically changed during pregnancy and lactation. It is derived from the changes in genes and hormones. Our results imply that changes in internal morphology and genes after a mouse gives birth might affect the thermal conductivity of the mammary gland, which will be discussed in detail in followed section.

The thermal conductivity of the mammary gland in pubertal mice is much lower than that of other organs reported in literature, such as 0.38 W m⁻¹ K⁻¹ for bovine liver^[36] and 0.89 W m⁻¹ K⁻¹ for mouth skin.^[37] Therefore, it is inaccurate to use the thermal conductivity of the mouse skin or other organs instead of that of the mammary glands for photothermal treatment analysis. Based on the thermal conductivity of the mammary gland in mice, the heat transferability of mammary gland could be characterized and the BC photothermal therapy could be explained from the perspective of thermal physics. The detailed thermal analysis of the mammary glands in pubertal mice is instrumental in improving photothermal therapy for more con-

venient and precise BC treatment. Combining accurate thermal properties and detailed numerical analysis helps precisely predict the photothermal therapy effectiveness. The thermal conductivity measurement of the mammary glands can be adapted to determine early symptoms of BC, which will benefit the efficacy of thermography-based diagnosis.

4.2. Explanations of Differences in Thermal Conductivity

As revealed in the experiments above, the mammary glands of mice with reproductive histories or not exhibit a distinct thermal conductivity disparity. The components of mammary glands need to be taken into consideration. The mammary gland is prominently composed of two portions: a ductal network formed by the bilayer mammary epithelium and its surrounding stroma, including adipocytes, vascular endothelial cells, stromal cells, and immune cells.^[38] In the nonlactating gland, white adipose tissue in the stroma comprises the majority of the mammary gland mass.^[39] Figure 2c and 2d shows the HE-stained slices of the mammary glands of the pubertal and mature mice. No obvious disparity in basic structure appears between two mammary glands in Paraffin tissue sections. However, the pubertal mammary gland is undergoing the process of epithelium expansion into the mammary fat pad through the proliferation of the terminal endbuds (TEBs). While the mature mice have completed the mammary development and experienced several cycles of the pregnancy-lactation-mature process. Thus, the epithelial cells and the surrounding tissue structure of the mammary glands go through a distinct amount of remodeling during each cycle.^[40]

Figure 5 illustrates a visualized comparison between the mammary ductal architecture of two groups of mice. In Figure 5a the ductal network of the pubertal mouse is incomplete, while in Figure 5b, an integrated ductal tree is shown in the mature mouse, which displays a higher density and number of mammary ducts than the former. It is readily comprehensible because the elevated level of hormones each time of pregnancy leads to a dramatic proliferation of epithelia by ductal side-branching and alveolar expansion. After lactation, the mammary gland turns into a mature state characterized by extensive epithelium apoptosis, adipose refilling, and tissue remodeling, which result in a state resembling the prepregnant mammary gland, but the ductal system retains more side-branching framework compared to the nulliparous mammary gland.^[41] The whole-mount-stained slices reveal less branching structure in puberty mammary ductal system than the mature one. Taking the results together, it can be concluded that the mammary gland of the mature mouse has a higher thermal conductivity, probably due to the changes in gland structure caused by the development and reproductive history. It indicates that thermal conductivity may differ individually and therefore could affect photothermal therapy.

5. The Role of Thermal Properties in Photothermal Therapy

5.1. Modeling Results and Discussion

Numerical simulations with finite element method have been conducted to further understand the role of thermal conductivity

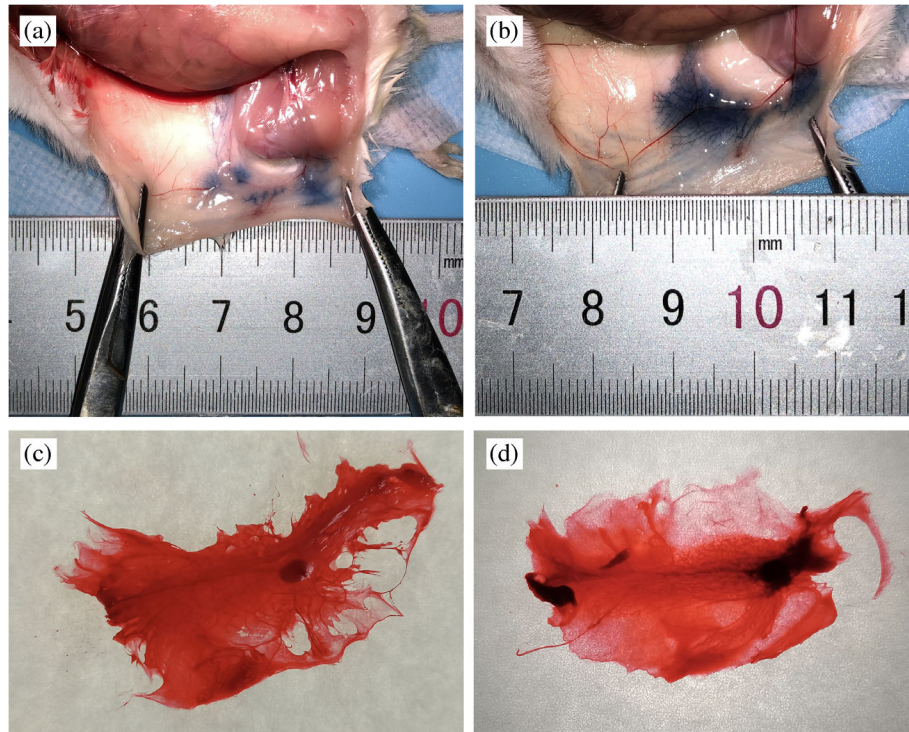


Figure 5. The inguinal mammary gland of a) pubertal mouse and b) mature mouse injected with methylene blue. The whole-mount stained mammary gland of c) the pubertal mouse and d) the mature mouse.

of mammary glands in pubertal and mature mice in photothermal therapy. The first stage of the simulation is to determine the physical model and relative governing equation of heat transfer in the mammary gland. Pennes bioheat transfer equation^[42] is commonly used to describe the interaction of biological tissue under laser irradiation. In this study, the heat radiation is ignored and the equation is described as

$$\rho c \frac{\partial T}{\partial t} = \nabla (k \nabla T) + \omega_b c_b \rho_b (T_b - T) + Q_{\text{met}} + Q \quad (3)$$

where ρ , c , k , and T denote the density, specific heat, thermal conductivity, and temperature of biomaterials, respectively. Then ω_b , c_b , ρ_b , and T_b denote the blood perfusion rate, specific heat, density, and temperature of the blood, respectively. The second term on the right side of the equation is the heat transfer from the blood. Q_{met} means the volumetric metabolic heat generation. The term Q represents the heat source of tissue converted from the absorption of light and it can be expressed as^[43]

$$Q(r, z, t) = \mu_a \varphi(r, z, t) \quad (4)$$

$$\varphi(r, z, t) = (1 - R) \varphi_0 \exp\left(-\frac{2r^2}{\omega_0^2}\right) \exp(\mu_s z) - \mu_t z \exp\left[-\frac{4(t - \tau)^2}{\tau^2}\right] \quad (5)$$

where μ_a , μ_s , and μ_t represent the absorption coefficient, scattering coefficient, and attenuation coefficient, respectively. $\varphi_0 = 2P_0/\pi\omega_0^2$ is initial luminous flux density, where P_0 denotes laser

power 150 mW. τ denotes irradiation time 300 s. The light intensity attenuates to P_0/e^2 where $r = \omega_0 = 0.4$ mm.

The simulation model is illustrated in **Figure 6a**. The mammary gland is supposed to be an axisymmetric geometric configuration. The experimental sample is set as a hexahedron of $0.5 \text{ cm} \times 0.5 \text{ cm} \times 0.12 \text{ cm}$. The heat convection would occur at the top surface ($z = 0$ mm) due to natural convection with the ambient air. A heat transfer coefficient of $4 \text{ W m}^{-2} \text{ K}^{-1}$ is considered to match the natural convection condition.^[44] The other surface boundary conditions are assumed to be at a constant surface temperature of 37°C . A core body temperature of 37°C is considered as the initial condition. The energy densities of line $y = 0$ along the x -axis at different depths (z -values) are shown in **Figure 6b**. A Gaussian distribution is presented along the radial direction (x -axis). The energy density decreases quickly along the z -axis, showing an exponential decay. The solving method of the equations is the finite element method, which has meshing advantages. The grid independence is checked for various grid sizes before calculation. There are only differences in the thermal properties of pubertal and mature mice. The optical properties, like incident conditions and other relative settings, are controlled as the same.

5.2. Simulation Results and Discussion

Temperature distributions at $z = 0$ mm plane are shown in **Figure 7a,b**. The models of pubertal and mature mice show a similar temperature distribution form under the same irradiation condition. The temperature at the center of the laser beam is the

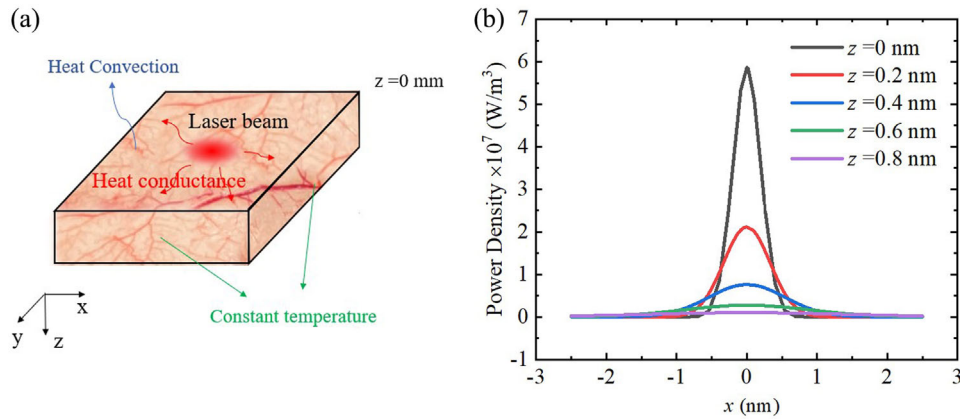


Figure 6. a) Numerical model and boundary conditions of simulation. b) Power density in different x–y plan.

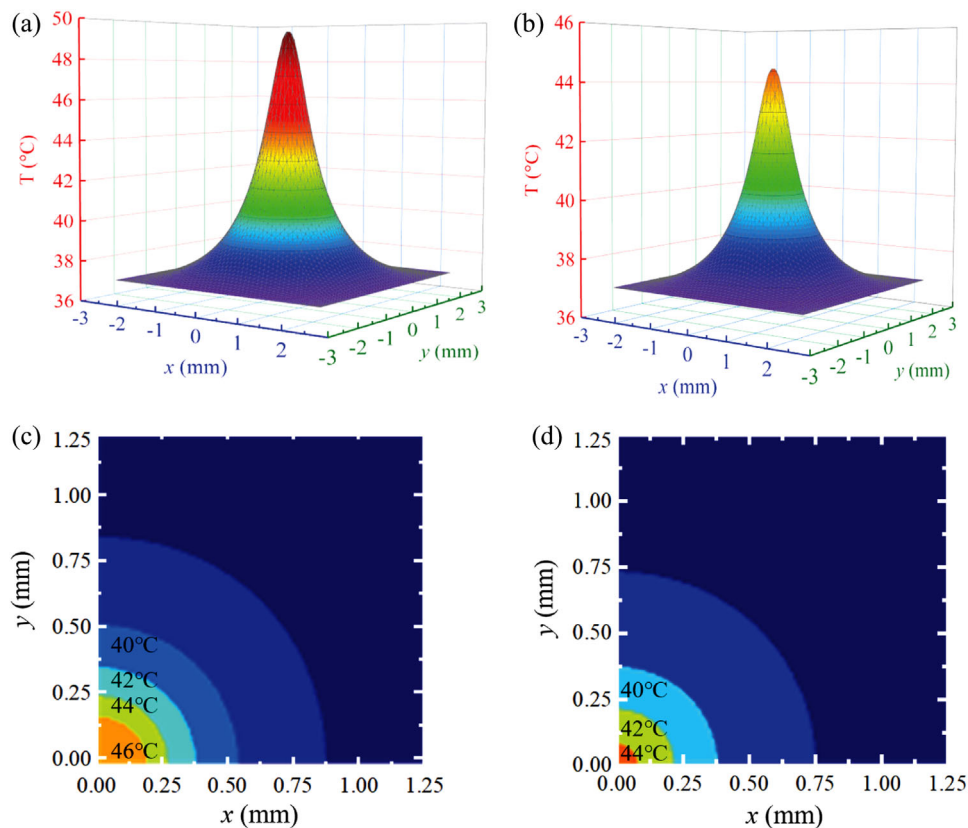


Figure 7. Temperature distribution at $z = 0$ mm of a) pubertal mice and b) mature mice. Quarter section temperature distribution at $z = 0$ mm of c) pubertal mice and d) mature mice.

highest, and then it decreases outward quickly. The maximum temperature of the pubertal mice tissue reaches 49.6 °C, which occurs at the point of incidence, whereas it is 44.6 °C for the mature mice. The pubertal mice have a higher temperature and sharper temperature decline radially than the mature mice due to the lower thermal conductivity.

Photothermal therapy requires elevating the tissue to 42–46 °C to take effect since protein denaturation and DNA damage occur in this temperature range. Thus, the area where the temperature

is above 42 °C is highly considered. For ease of expression, it is called an effective treatment area in this study. Since the temperature distribution is symmetrical, as shown in Fig 7a,b, a quarter section of the surface is analyzed for simplicity. As shown in Figure 7c,d, the temperature of a quarter section declines with the hemispherical radius. For the mammary gland in pubertal mice, the radius of the effective treatment area is about 0.375 mm, which means the cells in this area can be heated to ablate. For the mammary gland in mature mice, the radius of the effective

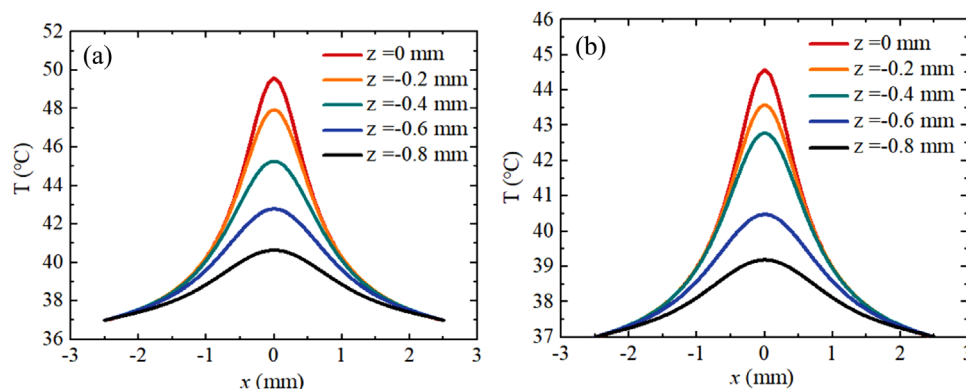


Figure 8. Temperature at different x - y plane of a) pubertal mice and b) mature mice.

treatment area is only 0.2 mm. The difference in the thermal conductivities reduced the effective treatment area of the mature mice by 21.7%. Hyperthermia requires an accurate temperature rise rate and distribution control to ablate target cells as a precise microscale treatment method. The damage to normal tissue is undesirable in photothermal therapy. A small effective treatment area could help to avoid damaging normal tissues. Thus, the mature mice can achieve a more accurate treatment than pubertal mice under the same irradiation conditions.

Besides the incident surface, we further study the treatment effects within the tissue. The temperature distributions of line $y = 0$ mm along the x -axis in the tissue of the pubertal and mature mice are shown in **Figure 8**. At each depth, the temperature declines with the distance from the incident point increase. The same form as power density distribution (Figure 6b) illustrates the temperature rise results from incident light. T_{\max} is different at each depth, and it declined with the depth increase. From $z = -0.2$ mm to $z = -0.4$ mm, the temperature in the tissue of the mature mice dropped faster than that in the pubertal mice. While from $z = -0.4$ mm to $z = -0.6$ mm, the result is conversible. The temperature in the tissue of the pubertal mice dropped more compared to that of the mature mice. In clinical application, photothermal therapy should consider the position of the tumor to take effects. The effective treatment depth ($T_{\max} > 42^\circ\text{C}$) is 0.6 mm for the mammary gland in the pubertal mice and 0.4 mm for the mature mice. Hence, the pubertal mouse can achieve better treatment of deeper tumors under the same illuminate conditions.

The simulation results demonstrate that the obvious differences will occur in the mammary glands' treatment effectiveness due to the difference of thermal conductivity in mammary glands using the same irradiation conditions. It is necessary and worthy to consider age and pregnancy in photothermal therapy.

6. Conclusion

In summary, for the first time, we measure the thermal conductivity of mammary glands in pubertal and mature mice with a customized method. The thermal conductivity of the mammary gland plays a key role in the effectiveness of BC clinical hyperthermia applications. It is measured to be $0.19^{+0.005}_{-0.005} \text{ W m}^{-1} \text{ K}^{-1}$ for the pubertal mice and $0.32^{+0.004}_{-0.004} \text{ W m}^{-1} \text{ K}^{-1}$ for the mature mice,

respectively, exhibiting 66.84% increment due to the microstructure differences. In addition, the role of thermal properties in clinical thermal therapy is further uncovered by the simulation analysis based on the experimental results. Under the same incident conditions, the different effectiveness in photothermal treatment between pubertal and mature mice is explored. Results show that the mammary glands in the pubertal mice exhibit a higher temperature rise and a deeper treatment area than the mature mice. Thus, mature mice need a more focused heating source to heat a smaller area to avoid damaging normal tissue and achieve accurate treatment compared to pubertal mice. The results imply that applying the same laser conditions to conduct hyperthermia is not appropriate for various types of patients, and at least, the role of reproductive history of patients should also be considered.

Acknowledgements

Y.F., W.Z., and Y.P. contributed equally to this work. The work was jointly supported by National Key Research and Development Program (No. 2019YFE0119900), Natural Science Foundation of Hubei Province (Innovative Group Project, 2020CFA026), National Natural Science Foundations of China (No. 52076156), and Fundamental Research Funds for the Central Universities (Nos. 2042020kf0194 and 2042019kf0229). The authors appreciate the support from the Supercomputing Center of Wuhan University.

Conflict of Interest

The authors declare no conflict of interest.

Data Availability Statement

Research data are not shared.

Keywords

mammary glands, photothermal therapy, thermal conductivity

Received: November 3, 2021
Revised: December 14, 2021
Published online: March 11, 2022

- [1] C. E. DeSantis, J. Ma, M. M. Gaudet, L. A. Newman, K. D. Miller, A. Goding Sauer, A. Jemal, R. L. Siegel, *Ca-Cancer J. Clin.* **2019**, *69*, 438.
- [2] F. Bray, J. Ferlay, I. Soerjomataram, R. L. Siegel, L. A. Torre, A. Jemal, *Ca-Cancer J. Clin.* **2018**, *68*, 394.
- [3] A. Walther, A. H. E. Muller, *Chem. Rev.* **2013**, *113*, 5194.
- [4] T. D. Schladt, K. Schneider, H. Schild, W. Tremel, *Dalton Trans.* **2011**, *40*, 6315.
- [5] H.-H. Lin, H.-W. Lee, R.-J. Lin, C.-W. Huang, Y.-C. Liao, Y.-T. Chen, J.-M. Fang, T.-C. Lee, A. L. Yu, H.-C. Chang, *Small* **2015**, *11*, 4394.
- [6] X. Bai, J. Ni, J. Beretov, P. Graham, Y. Li, *Cancer Treat. Rev.* **2018**, *69*, 152.
- [7] J. Dittmer, *Semin. Cancer Biol.* **2018**, *53*, 59.
- [8] D. Kumar, S. Singh, N. Sharma, K. N. Rai, *Int. J. Therm. Sci.* **2018**, *133*, 320.
- [9] Q. Ban, T. Bai, X. Duan, J. Kong, *Biomater. Sci.* **2017**, *5*, 190.
- [10] M. A. Miller, *Sci. Transl. Med.* **2018**, *10*, eear7512.
- [11] L. M. Martínez, D. Jaque, B. del Rosal, *Nanoscale* **2014**, *6*, 9494.
- [12] D. P. O'Neal, L. R. Hirsch, N. J. Halas, J. D. Payne, J. L. West, *Cancer Lett.* **2004**, *209*, 171.
- [13] M. Simon, K. Norregaard, J. T. Jorgensen, L. B. Oddershede, A. Kjaer, *Int. J. Nanomed.* **2019**, *14*, 5369.
- [14] Y. Zou, M. L. Li, T. Xiong, X. Z. Zhao, J. J. Du, J. L. Fan, X. J. Peng, *Small* **2020**, *16*, 11.
- [15] K. Y. Park, H. S. Han, J. Y. Hong, S. J. Seo, S. J. Lee, *Dermatol. Ther.* **2020**, *33*, e13189.
- [16] O. Akhavan, E. Ghaderi, *Small* **2013**, *9*, 3593.
- [17] Z. Heidari, M. Salouti, R. Sariri, *Nanotechnology* **2015**, *26*, 195101.
- [18] J. Xamán, L. Lira, J. Arce, *Appl. Therm. Eng.* **2009**, *29*, 617.
- [19] C. S. Sanjaya, T.-H. Wee, T. Tamilselvan, *Appl. Therm. Eng.* **2011**, *31*, 1566.
- [20] E. Kapiainen, M. K. Kihlstrom, R. Pietila, M. Kaakinen, V.-P. Ronkainen, H. Tu, A. Heikkinen, R. Devarajan, I. Miinalainen, A. Laitakari, M. Ansarizadeh, Q. Zhang, G.-H. Wei, L. Ruddock, T. Pihlajaniemi, H. Elamaa, L. Eklund, *Cancer Res.* **2021**, *81*, 129.
- [21] W. J. Parker, R. J. Jenkins, C. P. Butler, G. L. Abbott, *J. Appl. Phys.* **1961**, *32*, 1679.
- [22] F. Leresche, L. Ludvikova, D. Heger, U. von Gunten, S. Canonica, *Environ. Sci. Technol.* **2020**, *54*, 15057.
- [23] M. F. Cawley, P. A. Mooney, P. O'Connor, *Int. J. Heat Mass Transfer* **2008**, *51*, 224.
- [24] N. C. Bhavaraju, H. Cao, D. Y. Yuan, J. W. Valvano, J. G. Webster, *IEEE Trans. Biomed. Eng.* **2001**, *48*, 261.
- [25] S. N. Schiffres, J. A. Malen, *Rev. Sci. Instrum.* **2011**, *82*, 064903.
- [26] S. Roy-Panzer, T. Kodama, S. Lingamneni, M. A. Panzer, M. Asheghi, K. E. Goodson, *Rev. Sci. Instrum.* **2015**, *86*, 024901.
- [27] S. Krause, A. Brock, D. E. Ingber, *J. Vis. Exp.* **2013**, *1*.
- [28] N. Shalkevich, W. Escher, T. Buerger, B. Michel, L. Si-Ahmed, D. Poulidakos, *Langmuir* **2010**, *26*, 663.
- [29] A. Bhattacharya, R. L. Mahajan, *Physiol. Meas.* **2003**, *24*, 769.
- [30] O. Dyck, S. Jesse, N. Delby, S. V. Kalinin, A. R. Lupini, *Ultramicroscopy* **2020**, *211*, 112949.
- [31] W. Ding, Z. Ji, C. Liu, R. Duan, *Appl. Phys. Lett.* **2021**, *118*, 023701.
- [32] S. Bhanushali, N. N. Jason, P. Ghosh, A. Ganesh, G. P. Simon, W. Cheng, *ACS Appl. Mater. Interfaces* **2017**, *9*, 18925.
- [33] G. Delhomme, W. H. Newman, B. Roussel, M. Jouvét, H. F. Bowman, A. Dittmar, *IEEE Trans. Biomed. Eng.* **1994**, *41*, 656.
- [34] B. M. Heckman-Stoddard, T. Vargo-Gogola, M. P. Herrick, A. P. Visbal, M. T. Lewis, J. Settleman, J. M. Rosen, *Dev. Biol.* **2011**, *360*, 1.
- [35] J. F. Kugel, J. A. Goodrich, *Trends Biochem. Sci.* **2012**, *37*, 144.
- [36] G. Delhomme, W. H. Newman, B. Roussel, M. Jouvét, H. F. Bowman, A. Dittmar, *IEEE Trans. Biomed. Eng.* **1994**, *41*, 656.
- [37] X.-L. Zhang, Y.-B. Wang, Z. Kai, S. Ting, *J. Refrig.* **2020**, *41*, 161.
- [38] S. Pamarthy, L. Mao, G. K. Katara, S. Fleetwood, A. Kulshreshtha, A. Gilman-Sachs, K. D. Beaman, *Cell Death Dis.* **2016**, *7*, e2443.
- [39] S. Landskroner-Eiger, J. Park, D. Israel, J. W. Pollard, P. E. Scherer, *Dev. Biol.* **2010**, *344*, 968.
- [40] C. Dravis, C.-Y. Chung, N. K. Lytle, J. Herrera-Valdez, G. Luna, C. L. Trejo, T. Reya, G. M. Wahl, *Cancer Cell* **2018**, *34*, 466.
- [41] J. L. Fendrick, A. M. Raafat, S. Z. Haslam, *J. Mammary Gland Biol. Neoplasia* **1998**, *3*, 7.
- [42] H. H. Pennes, *J. Appl. Physiol.* **1998**, *85*, 5.
- [43] A. P. Mosk, A. Lagendijk, G. Lerosey, M. Fink, *Nat. Photonics* **2012**, *6*, 283.
- [44] B. Choi, J. A. Pearce, A. J. Welch, *Phys. Med. Biol.* **2000**, *45*, 541.